NATIONAL AERONAUTICS AND SPACE ADMINISTRATION

Technical Memorandum 33-506

Low-Acceleration Solid-Propellant Rocket Ignition Study

Leon D. Strand

JET PROPULSION LABORATORY
CALIFORNIA INSTITUTE OF TECHNOLOGY
PASADENA, CALIFORNIA

December 1, 1971

NATIONAL AERONAUTICS AND SPACE ADMINISTRATION

Technical Memorandum 33-506

Low-Acceleration Solid-Propellant Rocket Ignition Study

Leon D. Strand

JET PROPULSION LABORATORY
CALIFORNIA INSTITUTE OF TECHNOLOGY
PASADENA, CALIFORNIA

December 1, 1971

Prepared Under Contract No. NAS 7-100
National Aeronautics and Space Administration

PREFACE

The work described in this report was performed by the Propulsion Division of the Jet Propulsion Laboratory.

ACKNOWLEDGMENT

The author is indebted to Mr. L. Ford for preparing the igniter and main motor propellant charges and Mr. A. Rasmussen and Mr. S. Roche for assistance with the test firings and instrumentation. Computer programming was performed by Mr. F. Robertson of Lockheed Technical Services.

CONTENTS

FIGURES (contd)

ABSTRACT

A study was conducted to develop a solid-propellant rocket igniter system that would build up thrust at a controlled rate of less than 0.2 g/s. The system consisted of a long burning, regressive burning, controlled flow igniter and an inhibited progressive burning surface in the main rocket motor. The igniter performed the dual role of igniting under vacuum back-pressure and low L^* conditions the nonrestricted portion of the propellant and providing the mass addition necessary to sustain combustion until the propellant burning area had increased sufficiently to provide a stable motor-chamber pressure. Two series of tests were conducted with existing small test motor hardware to (1) demonstrate the feasibility of the concept, (2) determine the important parameters governing the system, and (3) obtain design guidelines for future scaled-up motor tests. A quasi-steady-state mass balance for the ignition system was written and programmed for use as a motor design tool.

I. INTRODUCTION

Typical solid-propellant motors are ignited and build up thrust very rapidly (5-50 g/s); however, spacecraft such as those of the Mariner series cannot withstand high acceleration transients. Therefore, a solid rocket "g-dot" ignition system is sought that is capable of building up thrust at a controlled rate of less than 0.2 g/s. Three approaches were considered:

(1) To mount additional small solid-propellant motors on the spacecraft to give a precisely timed sequence of thrust.

(2) To use a variable-area throat (ablative or pintle nozzle) and inhibited progressive burning surface to maintain the motor chamber pressure above the low-pressure combustion instability limit.

(3) To use a long burning, regressive burning, controlled flow igniter and an inhibited progressive burning surface in the main rocket motor (see Fig. 1).

Approach (3) was selected as the best method, and a feasibility demonstration program was begun. The goals of the program were two-fold: (1) to show the feasibility of the concept and (2) to generate design data and guidelines for later scaled-up motor tests.

II. LOW-ACCELERATION IGNITION SYSTEM

The method is a new adaptation of the fluid control or mass excitation solid-propellant motor concept (Ref. 1), where the motor is designed to operate below its low-pressure L^* extinction limit when additional gaseous mass is injected into, or generated in, the motor chamber. A simplified mass-balance method of illustrating the approach to be discussed is shown in Fig. 2 (past experience has shown that a nonequilibrium condition such as the one illustrated occurs at lower pressures below the L^* (motor free volume/nozzle throat area ratio) pressure extinction boundary (Ref. 2). A certain percentage (in the 75-90% range) of the initial burning surface of an end-burner motor is covered with a rubber restricter. A regressive burning, controlled flow igniter then performs the dual role of igniting under vacuum back-pressure and low L^* conditions the nonrestricted portion of the propellant surface and of providing the mass addition necessary to sustain combustion at pressures below the L^* combustion limit throughout the low-pressure ignition transient period. Both the propellant burning area of the main motor and, consequently, the chamber pressure increase with time in a controlled manner as the burning surface advances under the restricted surface until the motor is ultimately able to sustain stable combustion without additional mass addition from the igniter motor. The ignition transient is, of course, completed when the burning propellant surface has increased so as to provide a stable motor-chamber pressure. Note that the regressive burning, controlled flow igniter motor is required only to ignite and burn the main motor below its L^* combustion limit.

Two series of tests were conducted: (1) low-acceleration ignition motor firings to (a) demonstrate the feasibility of the concept, (b) carry out engineering development of igniter motor propellant grain configuration, main motor propellant restricter configuration, etc., and (c) determine the effects of igniter mass flow rate magnitude and main motor initial pressure on the main motor pressure-time profile; and (2) a series of motor firings to measure the variation in the L^* extinction limit with decreasing igniter motor/main motor mass flow rate ratio. These data are required to size the minimum initial mass flow rate of the igniter motor required for desired initial motor pressure and L^* values.

III. TEST SYSTEM

It was thought that the important flight motor parameters to be simulated would be the minimum and maximum operating pressure levels, maximum rate of change of pressure, and main motor initial L^*. Representative values for these parameters are minimum and maximum operating pressure levels of 20 and 100 N/cm^2, respectively, maximum permissible rate of change of pressure of 30 $N/cm^2/s$, and main motor initial L^* of 2.5-3.8 m. However, it was not possible to use existing test hardware to attain the low L^* levels that would be characteristic of flight motor designs and still maintain the desired minimum and maximum operating pressure levels. Also, since the low-pressure combustion limits for the fairly highly aluminized propellants to be used were found in laboratory motor tests not to be a strong function of L^* (Fig. 3), L^* simulation was not attempted in the first test series.

Figure 4 is a cross-sectional view of the major components of the test system. Existing test hardware was extensively used. The main motor is a 12.7 cm-ID by 15.2 cm-long Jet Propulsion Laboratory (JPL) batch check motor. For the first test series, end-burning case-bonded propellant charges were cast and pressure-cured in the motor chambers and then machined to a web thickness of 3.8 cm. The restricter configuration was cut from V-52 rubber (General Tire and Rubber Company) that had been cured to the desired thickness, and was bonded to the propellant surface with cement (Armstrong Products Co., Inc.). The initial free volume of the motor was approximately 8×10^{-4} m^3.

The igniter motor is a 7.6 cm-ID by 10.2 cm-long L^* — instability test motor. Two propellant charge configurations were used: a cantilevered cylinder restricted on both ends, and a regressive end burner (Figs. 4 and 5). The end-burner charges were prepared by machining the propellant charges to give the desired pressure-time curves and potting the charges in 6.35-cm-ID micarta tubes (Fig. 5). The cantilevered cylinder was ignited with the standard test-motor squib-igniter pellet system. The end burners used a pyrotechnic paste initiator system (Fig. 5). The technique is used to rapidly ignite acoustic T-burner propellant grains (Ref. 3). The initiator consisted of a fuse wire imbedded in a tablet of dried pyrotechnic paste. After the propellant surface to be ignited was painted with the paste, the tablet was glued to the surface.

The motors were fired into the JPL solid propellant test cell vacuum tank facility (Fig. 6). A back pressure of approximately 0.14 N/cm^2 was maintained for the tests. A copper vacuum diaphragm placed over the nozzle outlet maintained atmospheric pressure in the igniter motor until ignition occurred.

Test instrumentation consisted of two absolute pressure transducers (Statham Instruments, Inc.) on the main motor and one gage pressure (Taber Instrument Corp.) on the igniter motor.

IV. TEST SERIES 1

Key information about the igniter and main motors for the tests is listed in Table 1. The main motor propellant, a JPL formulation called Saturethane, has a saturated polybutadiene binder, an ammonium perchlorate oxidizer, and 16% aluminum. The oxidizer grains used either a non-aluminized Saturethane propellant or a polyether polyurethane binder propellant with 2% aluminum, as shown. The numerical test results are given in Table 2. The goals and results for each test are summarized here.

A. Test 1

The heat losses in the motor were apparently rather high and, as a result, in this first test firing, the igniter pressurized the main motor to a maximum pressure of only 1-2 N/cm^2. The igniter burned out without igniting the main motor charge, probably because the motor pressure generated by the igniter was below the low-pressure deflagration limit (P_{dl}) of the propellant.

B. Test 2

To ensure ignition of the main motor, the igniter mass flow rate was increased almost an order of magnitude over that of Test 1. The igniter pressurized the main motor to an initial pressure of approximately 38 N/cm^2. The motor pressure continued to rise in an expected manner to a maximum value of 95 N/cm^2, at which time the motor safety diaphragm unexpectedly burst, causing the pressure to drop to 45 N/cm^2. The motor then burned erratically (chuffed) until all of the propellant was consumed.

C. Test 3

The igniter mass flow rate was reduced approximately 20% over that of Test 2 in hopes of dropping the initial motor pressure into the desired region. The propellant restricter configuration for the main motor was similar to that illustrated in Fig. 4.

The resultant pressure-time traces for the igniter and main motor are reproduced in Fig. 7. Smooth curves were drawn through the plotted points; i.e., no attempt was made to reproduce any pressure irregularities.

The main motor was initially pressurized to 15 N/cm^2 by the igniter. Coincident with the igniter chamber filling to its equilibrium pressure level, the motor pressure rose at a rate of approximately 45 $N/cm^2/s$ to a value of 40 N/cm^2. The rate of rise then leveled off to a value of 6 $N/cm^2/s$. The loss of sonic flow in the igniter motor at an igniter motor pressure of approximately 120 N/cm^2 produced a corresponding drop in the main motor pressure. The maximum rise rate following recovery was approximately 17 $N/cm^2/s$. A maximum pressure of 110 N/cm^2 was attained. At 11 s from ignition, after the maximum propellant burning area had been reached, the dislodged restricter segments clogged the nozzle throat, causing the motor safety diaphragm to burst. The motor continued burning at a reduced pressure until propellant burnout. Some low-frequency, low-amplitude oscillations in the main motor pressure were evident during the initial several seconds of the test.

Because of the rapid pressurization of the motor by the igniter, it was difficult to deduce exactly when ignition in the main motor did occur. The test did illustrate the importance of delaying loss of sonic flow in the igniter motor nozzle or burnout of the igniter motor until most of the main motor pressurization is being produced by the main motor itself.

D. Test 4

The goals in Test 4 were to investigate the effects of reducing the initial main motor pressure further and to use an igniter of longer duration that would continue to flow sonically until its propellant was consumed. The regressive end-burner propellant charge used in the igniter is shown in Fig. 5. The main motor restricter configuration used in this and all succeeding g-dot ignition tests is shown in Fig. 8. It was thought that this new configuration would allow more rapid flame spreading over the unrestricted propellant surface and would have less tendency to pull away from the chamber and block the nozzle.

The test was highly successful. Smoothed pressure traces of the igniter and main motor are shown in Fig. 9. Post-test inspection revealed restricter segments wedged in the nozzle entrance, but no blocking of the nozzle. The main motor pressure again exhibited the low-frequency oscillations, this time over a fairly distinguishable interval of approximately 3.5 s. The oscillations, which appeared to begin at a chamber pressure of

approximately 12 N/cm^2, grew in amplitude with increasing pressure and reached a maximum of 19% of the mean pressure at a pressure of approximately 19 N/cm^2, then rapidly dampened out and approached zero at a pressure of approximately 30 N/cm^2. The very low amplitude oscillations appeared to continue as the pressure increased, but were difficult to distinguish from the erratic pressure perturbations and instrumentation "noise" that occurred throughout the run. The frequency of the oscillations grew from an initial value of 5 Hz to a value of 10 Hz at 20 N/cm^2. At their maximum amplitude the oscillations in pressure gave rates of change of pressure of 110-140 $N/cm^2/s$. These rates were much greater than the desired upper limit of 30 $N/cm^2/s$.

The fact that the main motor pressure began to oscillate independently in a nonacoustic fashion at a pressure of approximately 12 N/cm^2 indicates that ignition had occurred at or before this point. The initial L^* (free volume/nozzle throat area) of the main motor for this test was approximately 8.9 m. From the L^*-motor data (Fig. 3), the low-pressure combustion limit for aluminized Saturethane propellant at an L^* of 8.9 m is between 30 and 35 N/cm^2. It was concluded, therefore, that the feasibility of the g-dot ignition concept had been demonstrated, in that a motor was ignited below its low-pressure L^* combustion limit and successfully made the transition to the stable operating region in a controlled manner.

E. Test 5

The primary goal in Test 5 was to investigate the effect on the pressure oscillations of increasing the initial igniter motor mass discharge rate and, consequently, the initial main motor pressure. The initial pressure value of 13 N/cm^2 was approximately double that of the previous test. The thickness of the restricter was also reduced from 0.64 cm to 0.25 cm in hopes that it would completely decompose during the test. The periodic oscillations appeared to develop immediately following ignition and to be dampened out when the pressure reached approximately 24 N/cm^2 (as in Test 4, the pressure trace was never completely smooth at any time during the test). The duration of the oscillations was reduced to less than 1 s. As expected, the maximum growth in the amplitude of the oscillations was also reduced, to a maximum of 10% of the mean pressure at a pressure of 17 N/cm^2. The maximum oscillatory rate of change of pressure dropped

to 70 N/cm^2. The thinner propellant restricter performed as desired, as no traces of the restricter could be found in the motor after the test firing.

F. Test 6

Test 6 was designed to demonstrate that combustion cannot be sustained in the main motor without mass addition from the igniter motor until the main motor burning area has increased sufficiently. The igniter was sized to provide an initial main motor pressure of 20 N/cm^2 and to have a burning duration of 0.3 to 0.4 s. The pressure traces for the test are shown in Fig. 10. The igniter-chamber-filling process occurred over most of the igniter duration. The large free volume in this igniter made the pressure differential greater than normal. The main motor pressure followed the igniter pressure throughout the test, rising to a maximum level of 51 N/cm^2 and then tailing off with the igniter tail-off. A post-test view of the main motor propellant surface is shown in Fig. 11. Close inspection of the surface revealed that the propellant surface had begun to recede under the restricter and had therefore indeed been burning. The still small burning area was unable to sustain combustion after burnout of the igniter motor.

G. Test 7

For each run, a calculation of the c* value was made by using the conditions at the point of peak igniter pressure. This point occurred about 1 s after ignition, where the conditions should have reached a quasi-steady state, but where the igniter and main motor burning areas could still be roughly approximated by their pre-ignition values. The c* values were calculated by using the following steady-state mass balance equation for the overall motor chamber at any given time:

$$\dot{m}_{ig} + \dot{m}_{motor} = \frac{P_c A_t g}{c^*} \tag{1}$$

where

$\dot{m}_{ig}$ = the igniter mass discharge rate

$= (A_b \rho r)_{ig}$

$\dot{m}_{motor}$ = gas generation in main motor

$= (A_b \rho r)_{motor}$

A_b = unrestricted propellant burning area

ρ = propellant density

r = propellant regression rate

P_c = the main motor chamber pressure

A_t = the main motor nozzle throat area

c^* = the main motor characteristic velocity

g = gravitational constant

The calculated c^* values varied between 760 and 900 m/s. Since the values were found to vary up to 60 m/s with small changes in the main motor pressure chosen, the results are usable only for rough comparison. The theoretical low chamber-pressure (70 N/cm^2) c^* value for both the igniter and main motor propellants is approximately 1500 m/s, which is 40-50% higher than the values calculated from the test results. It was thought that this discrepancy was probably due to heat losses to the heavy steel aft-closure of the motor. Since the final goal of this work is to provide design data for larger, flight-weight motors, a test was performed to verify this.

The interior surface of the motor aft-closure was insulated with approximately a 0.6 cm-thick layer of V-61 material. The igniter burning area for this test was raised slightly from that of Test 5. The insulated closure had an appreciable effect on the test results. The ratio of the initial main motor and igniter pressures was 50% higher than the values for the previous three tests. Through the use of Eq. (1), a c^* value of 1460 m/s was calculated from the test data. This result indicates that theoretical propellant c^* values should be able to be used in preliminary-type calculations to size igniters for insulated, flight-type, solid-propellant rocket motors.

H. Test 8

In attempts to apply laboratory motor L^*-P_c extinction data in the design of larger extinguishable solid-propellant rockets, a motor-size scaling effect was found to exist (Ref. 4). The larger motors extinguished at lower pressures than would be predicted from the laboratory data; i.e., were more difficult to extinguish. Although both the 12.7 cm-diameter

motor used in these tests and the 7.6 cm-diameter motor used to obtain the L^*-extinction characteristics of the test propellant (Fig. 3) are small motors, a test was performed to obtain an extinction data point under motor conditions similar to those used in this program.

A regressive end-burner propellant charge was machined and potted in a 12.7 cm-diameter motor chamber, as shown in Fig. 12. The motor was fired into the vacuum tank, as in the previous tests. The pyrotechnic paste technique was used to ignite the 12.7 cm-diameter propellant surface.

The motor pressure reached a maximum of 90 N/cm^2 and continued to burn regressively until extinction occurred at a mean chamber pressure of 28 N/cm^2. Typical L^*-instability pressure oscillations for this type of test (low frequency, low amplitude) began rather abruptly at a motor pressure of 70 N/cm^2 and continued until extinction. The frequency of the pressure oscillations prior to extinction was 8 Hz. The post-test motor free volume was measured at 1×10^{-3} m^3, resulting in an extinction L^* of 11 m. At this L^* value the 7.6-cm motor data of Fig. 3 would predict a mean extinction pressure of 31 N/cm^2. This difference is within the scatter in this type of data.

V. TEST SERIES 2

From Eq. (1), the initial main motor pressure is a function of the unrestricted propellant burning area, the motor nozzle throat area, and the igniter mass discharge rate. In any motor design the nozzle throat area would be fixed by the fully developed maximum chamber pressure desired. The effects of trade-offs in unrestricted burning area and igniter mass discharge rate were not systematically studied in the first test series, the unrestricted burning areas reported in Table 1 having been arbitrarily chosen. In the effort to minimize the required mass discharge rate, the mass balance criterion of Fig. 2 is inadequate, as it is a necessary, but not sufficient, condition for stable burning for motors in the low-pressure, low-L^* region.

It was shown experimentally (Ref. 1) that a reduction in the secondary fluid injection rate resulted in an increased minimum pressure limit for stable combustion, i.e., combustion instability and extinction occurred at higher motor chamber pressures. A series of motor firings was carried out to determine the effect of variation of the igniter motor to main motor propellant mass addition rates (the $\dot{m}_{ig}$ and $\dot{m}_{motor}$ terms of Eq. 1) on the main motor L^* instability and extinction limits. Their ratio, $\dot{m}_{ig}/\dot{m}_{motor}$, is analogous to the fluid-to-solid ratio of Ref. 1.

The test system was identical to that used for the first series of tests, with the exception that, instead of being cast directly, the main motor propellant grains were first machined to the desired configuration and then potted in the motor chamber with Ecco Bond No. 45 cement (Emerson & Cuming, Inc.). The propellants used were Saturethane and later a polyether polyurethane binder, 16%-aluminized formulation with a trimodal ammonium perchlorate oxidizer blended for reduced burning rate – pressure characteristics (JPL 540 J). Both propellants have similar low-pressure L^* extinction characteristics (Fig. 3) and, though not investigated in detail, in the 7.6 cm-ID motors their stability boundaries appeared to be near or greater than 70 N/cm^2 at the L^* conditions tested. To allow lower L^* values, the motor free volume was reduced by partially filling the motor aft-closure with V-61 material. The 2% aluminized polyurethane propellant of series 1 was used as the igniter propellant.

The test results are shown in Table 3. Initially the test system consisted of a regressive burning, main motor propellant grain (Fig. 8) and a neutral igniter motor. It was expected that, following ignition, the main motor pressure would decrease until L^* instability and eventually extinction occurred. Instead, in two of the three tests the $\dot{m}_{ig}/\dot{m}_{motor}$ ratio increased sufficiently with decreasing $\dot{m}_{motor}$ to enable the motors to continue burning stably until propellant burn-out.

The test system was then changed to a neutral main motor charge and a regressive igniter charge, resulting in a regressive main motor pressure-time history. For these tests the initial pressures following ignition in the main motor were held relatively constant in the low-pressure region (20-30 N/cm^2) desired for later scaled-up motor tests. By minimizing the test firing times and, consequently, the amount of main motor propellant consumed, better control of the main motor final L^* was also allowed. Tests were performed at initial L^* values of approximately 2.5 and 3.8 m. At an L^* of 2.5 m, neither of the main motor propellants could be properly ignited at the low pressures attempted (20-25 N/cm^2), even with $\dot{m}_{ig}/\dot{m}_{motor}$ values as high as 5.7. The motors would only chuff in a periodic manner until the igniter propellant was consumed.

At an initial L^* of approximately 3.8 m (using JPL 540 J propellant throughout) the motors were ignited at initial pressures in the 20-30 N/cm^2 range. In each test the main motor burned unstably (pressure oscillation frequencies of approximately 20 Hz) following ignition for approximately 1 s, extinguished, and then chuffed until the igniter propellant was consumed. A typical test pressure-time trace is shown in Fig. 13. With final L^*'s of approximately 4.0 m, the mean chamber pressure at extinction was found to be inversely proportional to the $\dot{m}_{ig}/\dot{m}_{motor}$ ratio, but rather weakly so (Fig. 14). Of perhaps greater consequence, the amplitudes of the pressure oscillations were found to decrease with increasing $\dot{m}_{ig}/\dot{m}_{motor}$ ratio, as shown in Table 3. It became apparent that in scaled-up motors with these relatively low L^* values, the igniter mass flow rates that would be required to completely eliminate instability in the 20-30 N/cm^2 region would require unacceptably large igniters. The tests were therefore not pursued to higher $\dot{m}_{ig}/\dot{m}_{motor}$ ratios. The initial main motor K_n values would also become so small that it was feared this might have some unforeseen effect.

VI. MASS BALANCE PROGRAM

In the design of an ignition system of this type for a motor, an igniter motor mass flow vs time profile and main motor propellant restricter configuration must be chosen that will give the desired main motor pressure-time profile. To assist in this task, the quasi-steady-state mass balance of Eq. (1) was programmed for solution on the IBM 1620 computer. An expression for the main motor's unrestricted burning area vs distance burned is first obtained for the desired restricter configuration. Imputing an igniter motor $\dot{m}$ vs time profile, the mass balance is then solved iteratively at fixed distance-burned intervals. At time zero (zero distance burned) the calculation assumes that the igniter and motor are completely ignited and at their initial equilibrium pressure conditions. An example of a typical main motor pressure-time calculation is shown in Fig. 15. The program has been useful as a trial-and-error design tool for helping determine the igniter motor output/main motor propellant restricter configuration combination required to give the approximate main motor pressure-time profile desired.

VII. SUMMARY AND CONCLUSIONS

The feasibility of the g-dot concept of controlling pressure build-up in a solid-propellant motor was demonstrated, in that small solid-propellant motors were ignited at pressures significantly below their low-pressure L^* extinction limit and brought up to design operating pressure in a controlled manner.

The ratio of the main motor and igniter nozzle throat areas was found to be an important design parameter. If the ratio is too large, as was the case in Test 1, an excessively large propellant burning area is required in the igniter to adequately pressurize the main motor. If the ratio is too low, as in Tests 2 and 3, it is difficult to design an igniter motor with a high enough chamber pressure-time history to ensure sonic nozzle flow throughout its burning time.

The important parameters in controlling the rate of pressure increase of the motor are the motor initial pressure, the regressive burning characteristics of the igniter motor and, of course, the propellant restricter configuration. The higher the initial pressure, the more rapidly the propellant will regress under the restricter and reach the steady-state burning area. The initial pressure of Test 7 was approximately five times that of Test 4, and the motor reached its maximum pressure value in one-half the time.

In Tests 4 and 5, the main motor clearly exhibited a fairly marked interval of low-frequency pressure oscillations below a chamber pressure level of roughly 30 N/cm^2. The oscillations were of sufficiently high amplitude to exceed the desired program g-dot constraints. The oscillation interval occurred below the L^* extinction pressure for the motor (Test 8 results).

Further tests showed this instability to be sensitive to the motor characteristic length L^* and the igniter motor to main motor propellant mass addition rates ratio $\dot{m}_{ig}/\dot{m}_{motor}$. Increasing the $\dot{m}_{ig}/\dot{m}_{motor}$ ratio depressed the motor L^* extinction pressure and reduced the amplitudes of the pressure oscillations, but the instability persisted at the L^* and motor pressure conditions investigated up to the highest $\dot{m}_{ig}/\dot{m}_{motor}$ ratios tested. As predicted from present L^* instability theories, Ref. 5 as an example, lowering the motor L^* increased the exponential growth rate

constant for the amplitude of oscillations, producing stronger pressure oscillations and chuffing. It was concluded that the burning time in the low-pressure instability region should be kept to a minimum, cutting down on the time for growth of the oscillation amplitudes.

In the first test series, irregular, nonperiodic pressure perturbations occurred in the main motor. They appeared to be superimposed upon the low-frequency instability and often continued to occur throughout the burning time of the motor. Post-fire examination of the motors always revealed a good deal of aluminum and alumina deposition on the nozzle inlet and throat regions. It has been concluded from previous small motor experience that such a build-up and sluffing off of solid material in the throat region can produce perturbations in the measured motor pressure. At present it is postulated that the irregular pressure oscillations experienced in this work have the same origin. Future scaled-up motor firings should help to clarify this question.

A quasi-steady-state mass balance expression, with an assumed motor c* efficiency of 90%, was extensively used as a tool for predicting the initial equilibrium pressure conditions in the insulated main motor and, to a lesser extent, for predicting the approximate main motor pressure-time history. This performance parameter is being used for preliminary g-dot ignition system design.

REFERENCES

1. Coates, R. L., Study of Fluid-Controlled Solid Propellant Rocket Motors (Restartable Solid, Variable Pulse (RSVP) Motor) (Title Unclassified), Final Report R-LPC-734-F. Lockheed Aircraft Corp., Propulsion Division, Redlands, Calif., Aug. 1967 (Confidential).

2. Strand, L. D., Summary of a Study of the Low-Pressure Combustion of Solid Propellants, Technical Report 32-1242, pp. 22-23. Jet Propulsion Laboratory, Pasadena, Calif., Apr. 15, 1968.

3. Perry, E. H., "T-Burner Studies," in Supporting Research and Advanced Development, Space Programs Summary 37-54, Vol. III, pp. 93-96. Jet Propulsion Laboratory, Pasadena, Calif., Dec. 1968.

4. Levinsky, C. T., and Kobalter, G. F., Feasibility Demonstration of a Single-Chamber Controllable Solid Rocket Motor, Quarterly Progress Report No. 4, RPL TR-66-164. Aerojet-General Corporation, Sacramento, Calif., June 1966 (Confidential).

5. Beckstead, M. W., and Price, E. W., "Nonacoustic Combustor Instability," AIAA J., Vol. 5, No. 11, pp. 1989-1996, 1967.

Table 1. Test Series 1: Igniter and main motor test information

(a) Igniter motor

Test	Initiator	Propellant type	Propellant configuration	Propellant weight, kg	Initial burning area, cm^2	Nozzle throat diam, cm
1	Pyrotechnic paste	Saturethane-0% Al	Regressive end burner	0.054	14.6	0.234
2	DuPont S-88 squib 20 B-KNO_3 pellets	Saturethane-0% Al	Cylinder	0.164	103	0.628
3	DuPont S-88 squib 20 B-KNO_3 pellets	Saturethane-0% Al	Cylinder	0.130	75.5	0.503
4	Pyrotechnic paste	Polyurethane-2% Al	Regressive end burner	0.105	18.3	0.318
5	Pyrotechnic paste	Polyurethane-2% Al	Regressive end burner	0.164	29.4	0.318
6	Pyrotechnic paste	Polyurethane-2% Al	Neutral end burner	0.018	43.2	0.318
7	Pyrotechnic paste	Polyurethane-2% Al	Regressive end burner	0.175	30.4	0.318
8	Main motor ignited directly by pyrotechnic paste system.					

Table 1 (contd)

(b) Main motor

Test	Propellant type	Propellant configuration	Propellant weight, kg	Propellant restricter	Initial burning area		Nozzle throat diam, cm	Initial K_n[a]	$\frac{(A_t)_{motor}}{(A_t)_{ig}}$[b]
					Area, cm^2	% of total			
1	Saturethane-16% Al	12.7 cm-diam end burner	0.820	8-36° pie segments, 0.64 cm thick	25.8	20	1.26	20	29
2	Saturethane-16% Al	12.7 cm-diam end burner	0.820	8-36° pie segments, 0.64 cm thick	25.8	20	1.10	27	3.1
3	Saturethane-16% Al	12.7 cm-diam end burner	0.867	6-45° pie segments, 0.64 cm thick	32.3	25	1.10	34	4.8
4	Saturethane-16% Al	12.7 cm-diam end burner	0.800	Fig. 8 configuration, 0.64 cm thick	17.4	14	1.10	20	12
5	Saturethane-16% Al	12.7 cm-diam end burner	0.809	Fig. 8 configuration, 0.25 cm thick	17.4	14	1.26	14	16
6	Saturethane-16% Al	12.7 cm-diam end burner	0.580	Fig. 8 configuration, 0.25 cm thick	17.4	14	1.10	20	12
7	Saturethane-16% Al	12.7 cm-diam end burner	0.816	Fig. 8 configuration, 0.25 cm thick	17.4	14	1.10	20	12
8	Saturethane-16% Al	Regressive end burner	0.300	None	123	100	1.10	140	--

[a]Ratio of propellant burning area to nozzle throat area.

[b]Ratio of nozzle throat areas of main motor to igniter motor.

Table 2. Test Series 1: Numerical test results

Test	$P_{igniter}$, N/cm^2		P_{motor}, N/cm^2		t_i, s[a]	Initial dP/dt, $N/cm^2/s$	Overall maximum dP/dt, $N/cm^2/s$
	Initial	Maximum	Initial	Maximum			
1		170		1.4			
2	141	160	38	96	2 Truncated	41	17
3	160	190	15	110	10	45	17
4	150	200	6.2	120	11 1/2	5.4	19
5	350	410	13	83	8 1/2	15	9.0
6	460	700	21	51	0.4		145
7	450	500	30	160	5 1/2	66	29

[a]Time between ignition and attainment of maximum main motor pressure.

Table 3. Test Series 2: Test information and results

Run	Motor propellant	Motor D_t, cm	$\frac{(A_t)_{motor}}{(A_t)_{ig}}$	Initial conditions following main motor ignition					
				Motor K_n	Motor L*, m	P_{motor}, N/cm^2	$\dot{m}_{ig}$, kg/s	$\dot{m}_{motor}$, kg/s	$\frac{\dot{m}_{ig}}{\dot{m}_{motor}}$
9	Saturethane	1.42	8	80	5.33	49	0.026	0.045	0.60
10	Saturethane	1.10	4.7	129	5.84	117	0.013	0.007	0.19
11	Saturethane	1.42	20	80	3.8	21	No data	0.023	No data
12	Saturethane	1.65	27.5	58	2.5	42	0.032	0.040	0.80
13	Saturethane	1.65	27.5	28	2.5	23	0.032	0.013	2.5
14	Saturethane	1.65	27.5	15	2.5	21	0.032	0.005	5.7
15	JPL 540 J	1.65	27.5	21	2.5	28	0.032	0.013	2.5
16	540 J	1.65	11	21	3.8	26	0.030	0.012	2.4
17	540 J	1.65	11	15	3.8	23	0.030	0.008	4.0
18	540 J	1.65	11	37	3.8	28	0.024	0.023	1.0

Table 3 (contd)

Run	Main motor extinction					Pressure oscillations		Comments
	Motor L*, m	P_{motor}, N/cm^2	$\dot{m}_{ig}$, kg/s	$\dot{m}_{motor}$, kg/s	$\frac{\dot{m}_{ig}}{\dot{m}_{motor}}$	Frequency, Hz	Total amplitude (av), N/cm^2	
9	6.1	34	0.010	0.035	0.3	6.7	3.8	Regressive igniter, motor extinguished.
10	7.1	38	0.013	0.015	0.9	Relatively stable		Regressive motor, motor burned until igniter burnout.
11	5.1	9.6	No data	0.003	No data	18	0.6	Regressive motor, motor burned until igniter burnout.
12	No data	23	0.014	0.025	0.55	15	5	Regressive igniter, motor extinguished and chuffed.
13	3.2					Chuffing		Regressive igniter, motor chuffed until igniter burnout.
14	2.5					Chuffing		Regressive igniter, motor chuffed until igniter burnout.
15	2.8					Chuffing		Regressive igniter, motor chuffed until igniter burnout.
16	3.9	21	0.025	0.010	2.5	20	1.5	Regressive igniter, motor extinguished and chuffed.
17	4.0	19	0.026	0.007	3.9	16	1.5	Regressive igniter, motor extinguished and chuffed.
18	4.2	23	0.018	0.019	0.95	17	3.5	Regressive igniter, motor extinguished and chuffed.

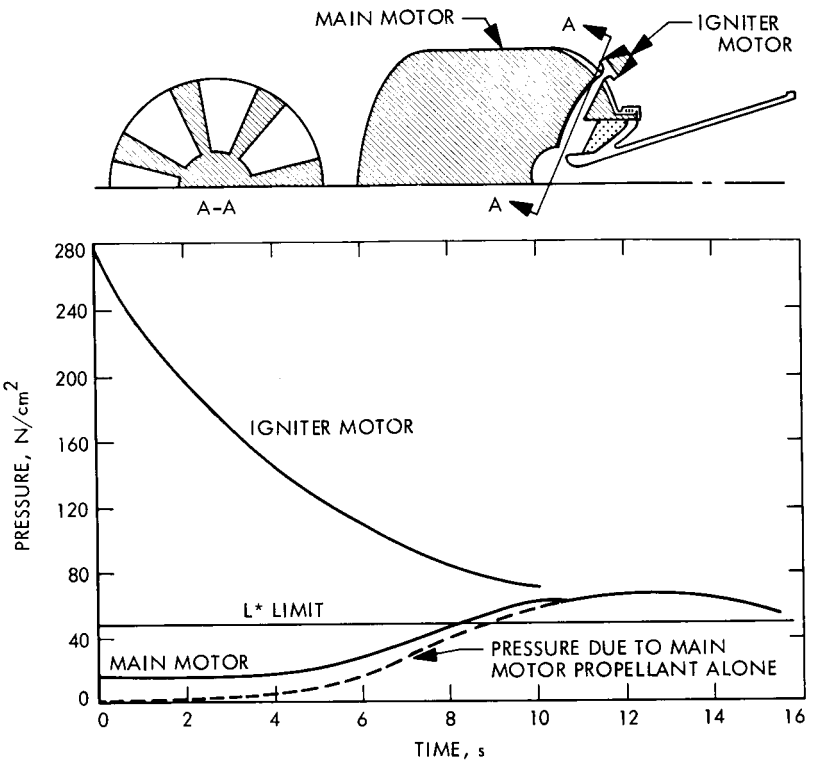

Fig. 1. Low-acceleration ignition concept

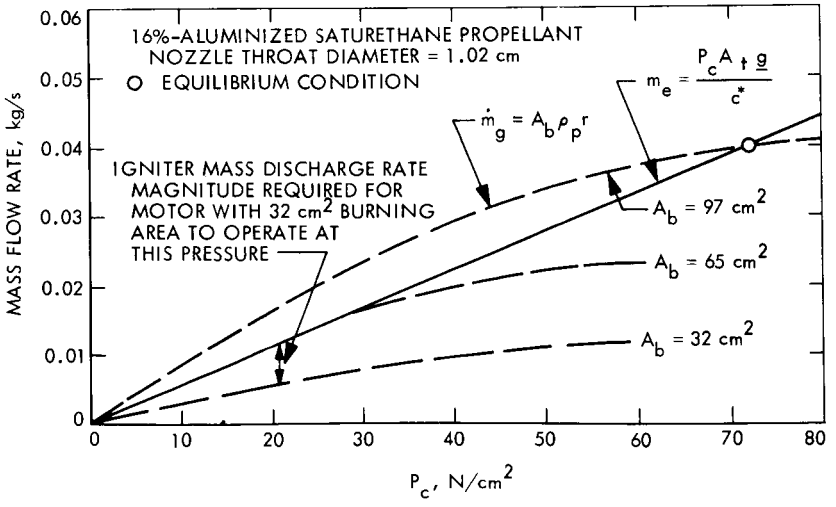

Fig. 2. Motor propellant gasification rate $\dot{m}_g$ and nozzle exhaust flow rate m_e vs motor chamber pressure, with motor propellant burning area A_b as independent parameter

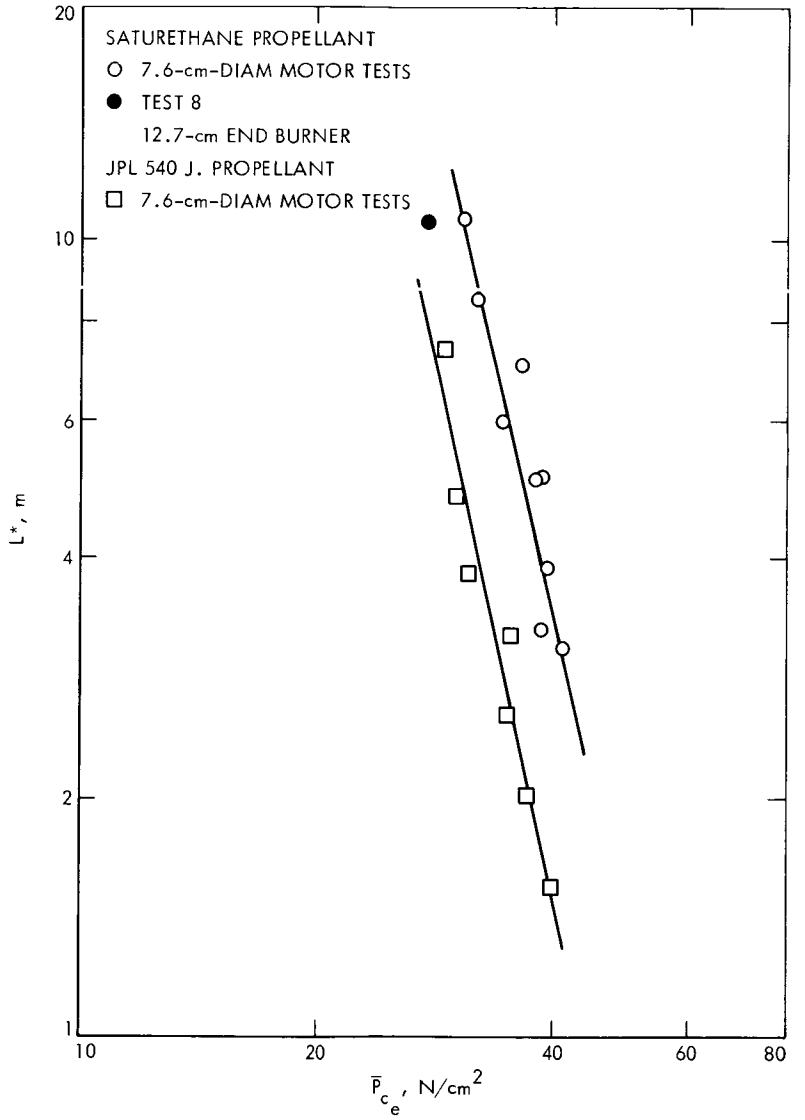

Fig. 3. L^* vs mean chamber pressure at combustion extinction

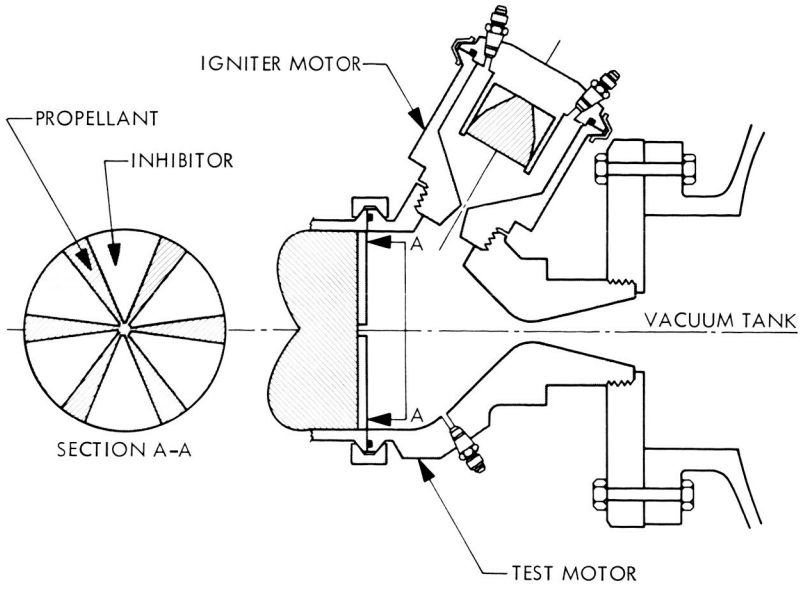

Fig. 4. Test system

Fig. 5. Igniter end-burner propellant charge, Test 4

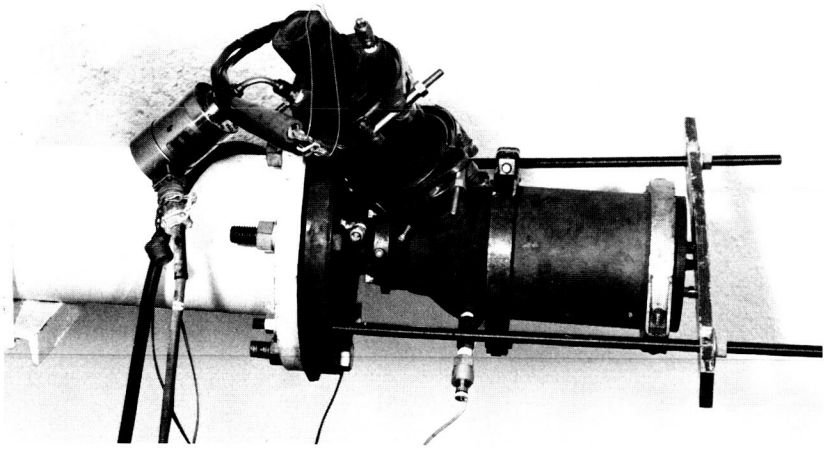

Fig. 6. Test system mounted on vacuum tank inlet pipe

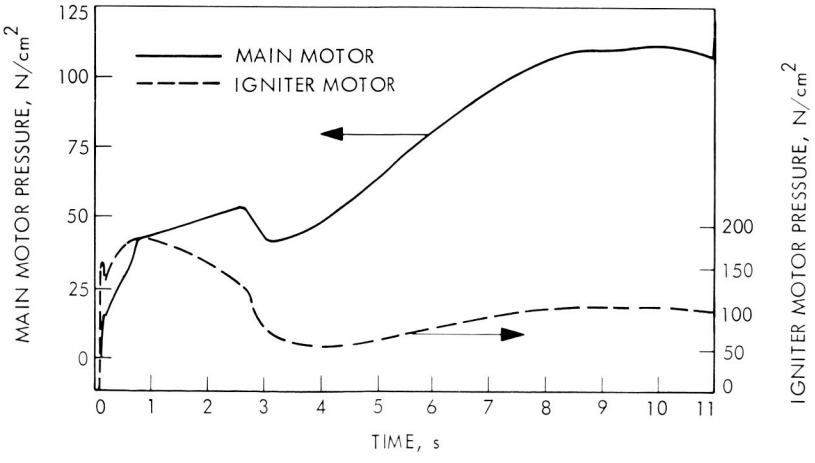

Fig. 7. Igniter motor and main motor test pressure-time traces, Test 3

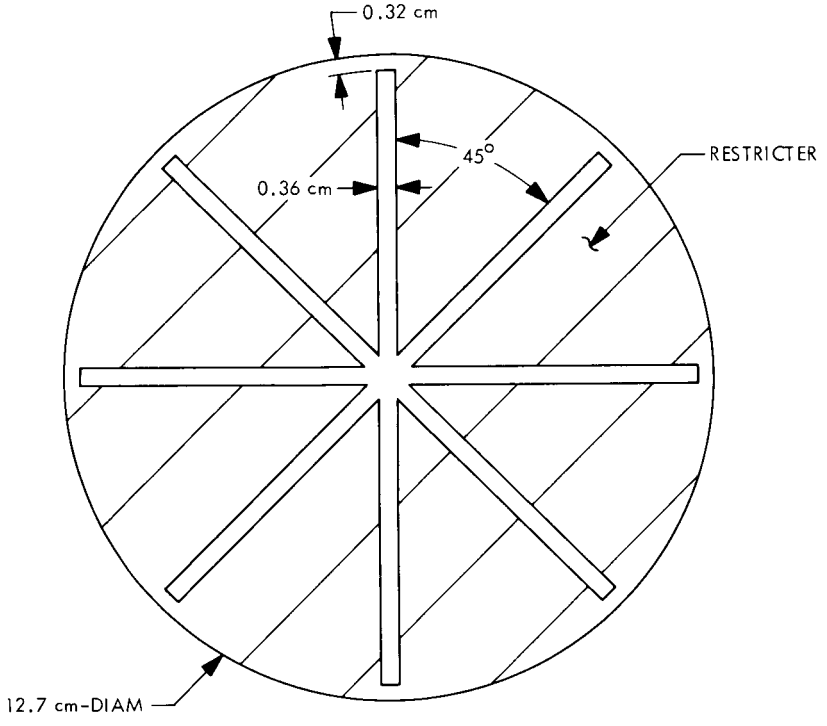

Fig. 8. Main motor propellant restricter configuration, Tests 4-7

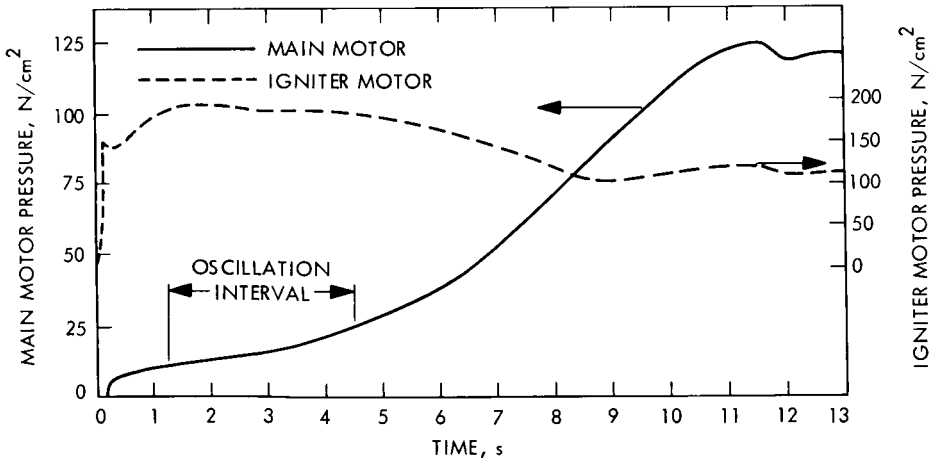

Fig. 9. Igniter motor and main motor test pressure-time traces, Test 4

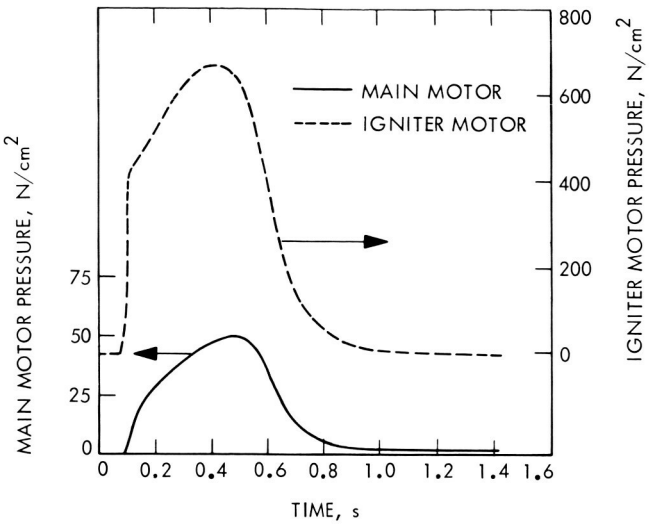

Fig. 10. Igniter motor and main motor test pressure-time traces, Test 6

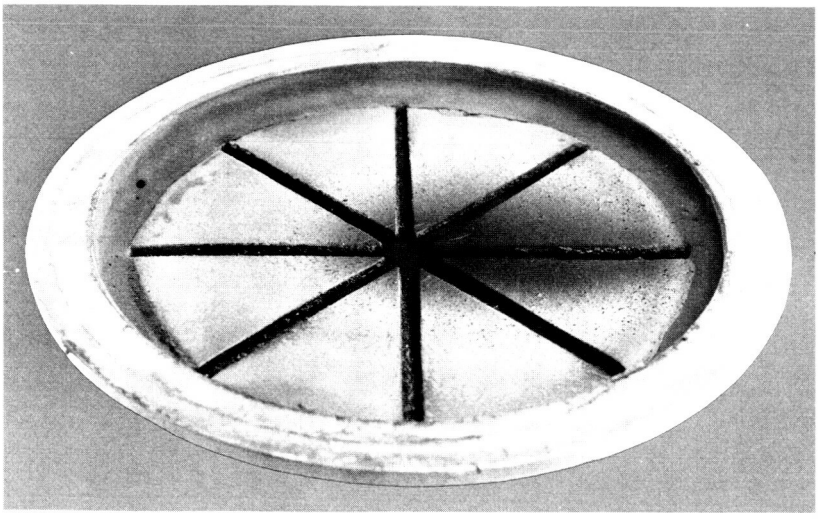

Fig. 11. Post-test view of main motor propellant surface, Test 6

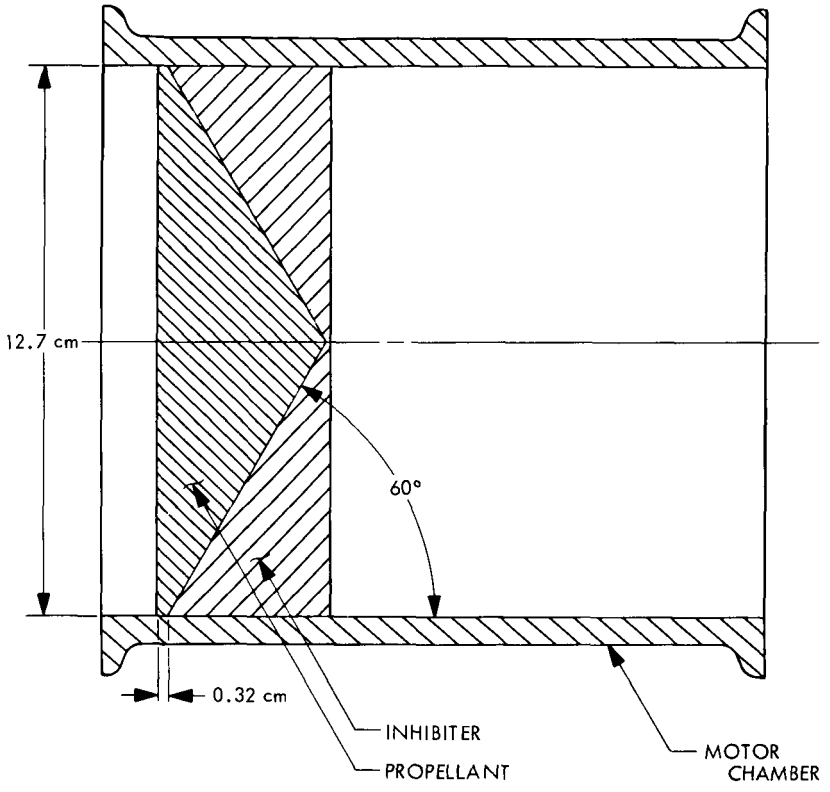

Fig. 12. Cross-section of regressive end-burner propellant charge, Tests 8, 10, and 11

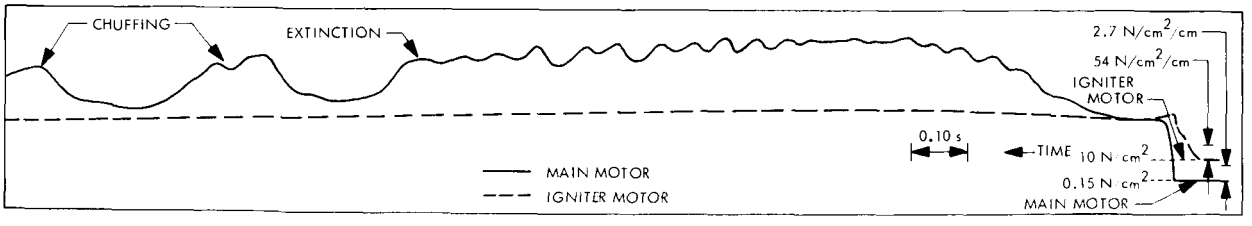

Fig. 13. Igniter and main motor pressure-time records, Test 16

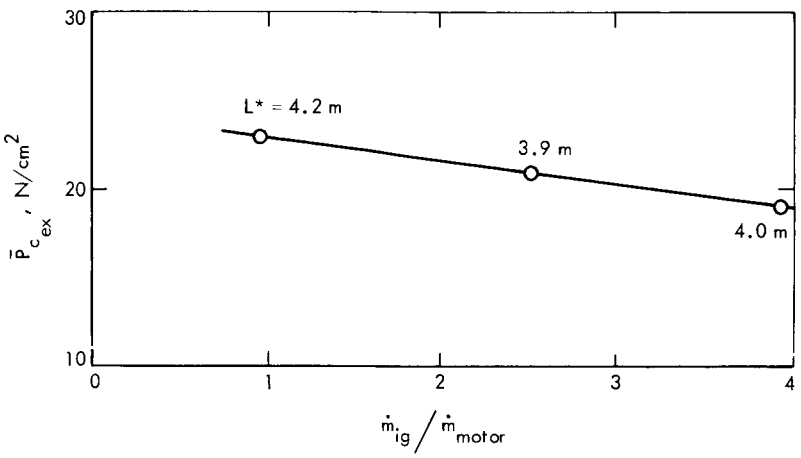

Fig. 14. Main motor mean pressure at combustion extinction vs ratio of igniter motor to main motor propellant mass addition rates

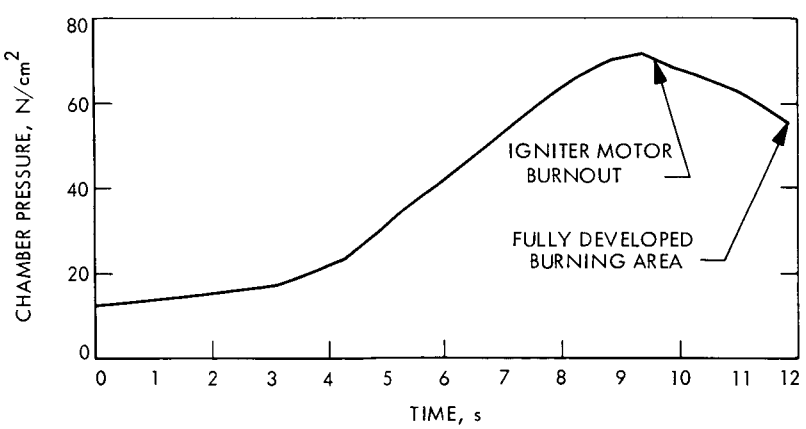

Fig. 15. Sample calculation: main motor mass balance computer program, main motor pressure vs time

NASA — JPL — Coml., L.A., Calif.